ACS Catalysis

pubs.acs.org/acscatalysis

Research Article

Influence of Promotion on the Growth of Anchored Colloidal Iron Oxide Nanoparticles during Synthesis Gas Conversion

N. A. Krans,[†] J. L. Weber,[†] W. van den Bosch, J. Zečević, P. E. de Jongh, and K. P. de Jong*

Cite This: *ACS Catal.* 2020, 10, 1913−1922

Read Online

ACCESS | Metrics & More | Article Recommendations | Supporting Information

ABSTRACT: Using colloidal iron oxide nanoparticles with organic ligands, anchored in a separate step from the supports, has been shown to be beneficial to obtain homogeneously distributed metal particles with a narrow size distribution. Literature indicates that promoting these particles with sodium and sulfur creates an active Fischer−Tropsch catalyst to produce olefins, while further adding an H-ZSM-5 zeolite is an effective way to obtain aromatics. This research focused on the promotion of iron oxide colloids with sodium and sulfur using an inorganic ligand exchange followed by the attachment to H-ZSM-5 zeolite crystals. The catalyst referred to as FeP/Z, which consists of iron particles with inorganic ligands attached to a H-ZSM-5 catalyst, was compared to an unpromoted Fe/Z catalyst and an Fe/Z-P catalyst, containing the colloidal nanoparticles with organic ligands, promoted after attachment. A low CO conversion was observed on both FeP/Z and Fe/Z-P, originating from an overpromotion effect for both catalysts. However, when both promoted catalysts were washed (FeP/Z-W and Fe/Z−P-W) to remove the excess of promoters, the activity was much higher. Fe/Z-P-W simultaneously achieved low selectivity toward methane as part of the promoters were still present after washing, whereas for FeP/Z-W the majority of promoters was removed upon washing, which increased the methane selectivity. Moreover, due to the addition of Na+S promoters, the iron nanoparticles in the FeP/Z(-W) catalysts had grown considerably during catalysis, while those in Fe/Z-P(-W) and Fe/Z(-W) remained relatively stable. Lastly, as a large broadening of particle sizes for the used FeP/Z-W was found, where particle sizes had both increased and decreased, Ostwald ripening is suggested for particle growth accelerated by the presence of the promoters.

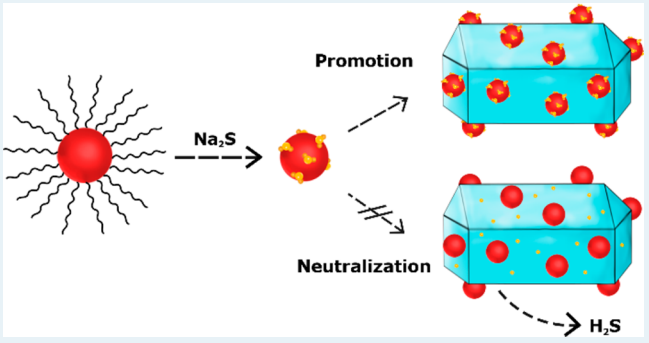

KEYWORDS: *colloidal nanoparticles, ligand exchange, promotion, Fischer−Tropsch to olefins and aromatics, iron-based catalysts, zeolites*

1. INTRODUCTION

Over recent years, research has focused on the exploration of alternative pathways to produce fuels and chemicals which are nowadays mainly obtained from oil. As a suitable replacement for oil, synthesis gas (a mixture of H_2 and CO) can be used, as it can be derived from natural gas, coal, CO_2, renewable hydrogen gas, and biomass[1−5] and can be converted to a wide range of products via monofunctional[6−8] and bifunctional catalysts.[9−11]

Recently, a bifunctional catalyst system has been introduced by the group of Prof. Bao consisting of a metal oxide and a zeolite (OX-ZEO) to convert synthesis gas to short olefins via reactive oxygenate intermediates such as methanol, dimethyl ether, or ketene.[9,12−14] The choice of zeolite material is crucial to control the resulting product spectrum of the OX-ZEO process. The reactive oxygenate intermediates can be converted to olefins using zeolites with small pore diameters such as SAPO-34 and SSZ-13. However, the use of a ZSM-5 zeolite owning a larger pore diameter allowed the formation of aromatics from these intermediates.[10,15]

Alternatively, synthesis gas can be converted in the Fischer−Tropsch synthesis (FTS) to ultraclean hydrocarbons in the range from methane to waxes.[6,16] Operating cobalt-based catalysts in the low-temperature Fischer−Tropsch process (LT-FTS) results in the formation of linear paraffins with high molecular weight, whereas the high-temperature Fischer−Tropsch synthesis (HT-FTS) using iron-based catalysts produces light olefins.[6,11,17,18]

The product spectrum of the FTS usually follows the Anderson−Schulz−Flory (ASF) distribution, a statistical distribution of products of surface polymerization reactions. However, adding promoters to an iron-based Fischer−Tropsch catalyst can lead to a deviation from the ASF distribution in the so-called Fischer−Tropsch to olefins (FTO) process.[19−22] The

Received: October 10, 2019
Revised: January 7, 2020
Published: January 8, 2020

presence of both sodium and sulfur promoters on the iron catalyst is essential for a decreased selectivity to methane and increased olefins/paraffin ratio.[23−25] This allows the formation of C_2-C_4 olefins with 65%$_C$ selectivity,[26] more than the ASF-predicted distribution of 58%$_C$ selectivity for the C_2-C_4 fraction (olefins plus paraffins).[27]

These short olefins being formed on the FTO catalyst with high selectivity can be further converted to aromatics on an H-ZSM-5 zeolite[28−30] not only starting from syngas but also using CO_2 as a reactant.[31] In this process, the Brønsted acid sites (BAS) of the zeolite enable the aromatization of olefins that are formed on the FTO catalyst. However, combining the zeolite and FTO catalyst promoted with sodium and sulfur can facilitate the migration of sodium ions from the FTO catalysts to the BAS of the zeolite. This results in zeolite acid site neutralization and a loss of the promotion effect of the FTO catalysts, thus increasing methane selectivity.[32]

Metal catalysts are typically prepared via methods such as incipient wetness impregnation (IWI) or precipitation.[33,34] These methods, however, can offer limited control over the metal particle size, shape, and distribution, which is of the utmost importance for catalyst activity, selectivity, and stability.[35−37] Therefore, research in academia has focused on colloidal synthesis methods which can controllably yield iron oxide nanoparticles (Fe-NP) of various sizes. Here, an iron precursor is decomposed at higher temperatures in a solvent in the presence of organic ligands, resulting in ligand stabilized Fe-NP in suspension. Colloidal particles are subsequently attached to different support materials, obtaining relatively sinter-resistant catalysts.[38−42]

Furthermore, model catalysts composed of colloidal iron nanoparticles supported on carbon nanotubes (CNT) were used to study the FTO reaction.[41,43] These colloidal particles were promoted with sodium and sulfur using an inorganic ligand exchange method.[44−46] Here, the organic ligands stabilizing the Fe-NP are (partially) replaced with inorganic ligands that can also act as promoters, such as Na_2S.[45,46] When applied in the FTO process, this exchange was performed after the Fe-NP were attached to the support material.[44] However, so far it has been challenging to direct the promoters so that they specifically attach to the iron particles and not to the support material.

Since the colloidal method has the advantage of controlling the particle size distribution, it means that it is easier to discern particle growth mechanisms.[24] Particle growth can be divided into two distinctively different mechanisms, namely Ostwald ripening, where the transport of mobile species happens over the support or in the gas phase, growing larger particles at the expense of smaller ones and coalescence and growth which involves particle migration over the surface, coalescing to form larger particles.[47]

In this study, we prepared colloidal Fe-NP and attached these in a separate step onto an H-ZSM-5 zeolite to convert synthesis gas to olefins and aromatics. This advanced synthesis method allows for uniform particle distributions where the particles are located on the exterior surfaces of the zeolite crystals. Using this method allows to create a catalyst which not only uses the ZSM-5 as a support but additionally to convert syngas into aromatics. To introduce sodium and sulfur promoters, inorganic ligand exchange with Na_2S was performed on the Fe-NP either before or after attachment onto the zeolite. These materials were used in the Fischer−Tropsch reaction to obtain olefins, which are further converted to aromatics. We show the influence of the synthesis sequence of Na+S promoted Fe-NP on H-ZSM-5 on the activity, selectivity, and stability. Using ligand exchange prior to the attachment (FeP/Z) compromised the catalyst stability when compared to ligand exchange after attaching the particles (Fe/Z-P). A washing step was used (FeP/Z-W and Fe/Z-P-W) to remove the excess of inorganic ligands which led to a more active catalyst for both promoted catalysts. Finally, analysis of the used catalyst revealed that particles from the promoted FeP/Z-W catalyst partially shrunk to smaller sizes than the fresh catalyst, giving a strong indication of the Ostwald ripening process.

2. EXPERIMENTAL SECTION

2.1. Catalyst Preparation. *2.1.1. Synthesis of 6 nm Iron Oxide Nanoparticles (Fe-NP).* All chemicals were obtained from Sigma-Aldrich unless stated otherwise. To synthesize the colloidal iron oxide nanoparticles, 0.43 g oleic acid (90% purity), 0.21 g oleylamine (70% purity), 0.35 g 1,2-hexadecanediol (≥98% purity) and 10 mL 1-octadecene (90% purity) were added to a three-neck round-bottom flask.[43] The reactants were degassed under vacuum in a Schlenk-line setup for 30 min 120 °C while magnetically stirring at 650 rpm. The stirring bar used in the preparations were glass-covered magnetic stirring bars to prevent contamination by iron uptake into the PTFE of conventional stirring bars. The suspension was subsequently purged with nitrogen gas, after which the temperature was lowered to 90 °C and a solution of 0.21 g iron pentacarbonyl (99.99%) in 1 mL 1-octadecene was injected. The temperature was then increased to 290 °C in 10 min, and the mixture was refluxed for 1 h. Subsequently, the obtained suspension of iron nanoparticles (Fe-NP) was cooled down to room temperature and further processed in air. The iron Fe-NP suspension was washed thrice, where the suspension was centrifuged in about 10 mL isopropanol at 2700 rpm for 15 min, and redispersed in five drops of toluene. Finally, particles were suspended in 2.4 mL of toluene by sonication for 5 min.

2.1.2. Attachment of Fe-NP onto H-ZSM-5. As-synthesized Fe-NP suspended in toluene were diluted with 10 mL 1-octadecene. 800 mg of powdered zeolite (H-ZSM-5, Zeolyst CBV 3024E, Si/Al = 15 at/at, calcined for 5 h at 550 °C in static air) was added to a 100 mL three-neck round-bottom flask, which was connected to a Schlenk line through a reflux cooler.[43] The suspended Fe-NP were added to H-ZSM-5 by pipetting while simultaneously magnetically stirring at 400 rpm. The mixture was brought under vacuum for 30 min at 120 °C to evaporate the toluene, and subsequently purged with nitrogen. The temperature was increased to 200 °C in 10 min under nitrogen flow and maintained for 30 min. Afterward, the mixture was cooled down to room temperature and further processed in air. Finally, the Fe-NP supported on the zeolite were washed five times with a mixture of *n*-hexane and acetone (1:3 v/v) and dried at 60 °C for 1 h under static air, at 120 °C for 3 h under static air, and at 80 °C for 3 h under vacuum. This method allowed the synthesis of Fe-NP attached to H-ZSM-5 zeolite with 3 wt % iron loading. These samples are referred to as Fe/Z.

2.1.3. Inorganic Ligand Exchange of Fe/Z. A 0.05 M sodium sulfide stock solution was obtained by sonicating 0.24 g sodium sulfide nonahydrate (≥98% purity) in 20 mL formamide (≥99.5% purity) for 1 h. 2.2 mL of the stock solution was added to 350 mg of Fe/Z and stirred at 400 rpm

https://dx.doi.org/10.1021/acscatal.9b04380
ACS Catal. 2020, 10, 1913−1922

for 10 min.[44] The promoted catalysts were first washed with ethanol, followed by four times washing with a mixture of ethanol and acetone (1:3 v/v), and finally washed with acetone. In every step, the supernatant was carefully decanted and pipetted off. Finally, the catalyst was dried at 60 °C for 1 h under static air, at 120 °C for 3 h under static air and at 80 °C for 3 h under vacuum. This promoted catalyst is designated as Fe/Z-P.

2.1.4. Inorganic Ligand Exchange of Fe-NP with Na_2S. For the direct promotion by inorganic ligand exchange, a method was adapted from A. Nag et al.[45] The as-synthesized Fe-NP suspended in toluene were added to 2.4 mL of a 0.5 M $Na_2S{\cdot}9H_2O$ solution in formamide. This formed two layers with the Fe-NP in toluene on top and the formamide solution at the bottom. The solution was vigorously stirred for 1 h. Afterward, the particles had transferred to the formamide layer. The particles were washed with acetonitrile, centrifuged at 2700 rpm for 15 min and redispersed in five drops of methanol three times. Finally, particles were suspended in 2.4 mL of methanol. These particles are denoted as FeP-NP.

2.1.5. Attachment of FeP-NP onto H-ZSM-5. FeP-NP suspended in methanol were added to 800 mg of the zeolite (H-ZSM-5, Zeolyst CBV 3024E, Si:Al = 15 at/at, calcined for 5 h at 550 °C in static air) in the Schlenk-line setup while stirring at 400 rpm. Slowly, the vacuum was applied to the suspension and it was heated to 50 °C to evaporate the methanol. The suspension was kept at these conditions for 1 h to ensure the FeP-NP had attached to the support. The catalyst was dried at 60 °C for 1 h under static air, at 120 °C for 3 h under static air, and at 80 °C for 3 h under vacuum. This catalyst is referred to as FeP/Z.

2.1.6. Washing Procedure. To remove the excess of sodium and sulfur promoters from the Fe-NP and to recover acidity of the zeolite by ion exchange, the catalysts (Fe/Z, Fe/Z-P, and FeP/Z) were washed with an ammonium nitrate solution. 400 mg catalyst was added to a 2 mL ammonium nitrate solution (1 mol/L in demineralized water) and stirred at 400 rpm and 25 °C for 1 h. Afterward, the catalysts were washed six times with a mixture of water and acetone (1:3 v/v), centrifuged and dried at 60 °C for 16 h. Catalysts will be referred to as Fe/Z-W, FeP/Z-W, and Fe/Z-P-W. After this procedure, the H-ZSM-5 had been converted into an NH_4-ZSM-5. However, during the in situ reduction at elevated temperatures the ammonia fully desorbed and the proton form of the zeolite was recovered, as evidenced by TPD (Figure S1 in the Supporting Information, SI). Moreover, the sample codes and descriptions of all catalysis have been explained in Table S1.

2.2. Catalyst Characterization. *2.2.1. Inductively Couple Plasma Atomic Emission Spectrometry.* The elemental composition of the catalysts was determined with a Thermo Jarrell Ash model ICAP 61E trace analyzer inductively coupled plasma atomic emission spectrometer (ICP-AES).

2.2.2. (Scanning) Transmission Electron Microscopy. To determine the size distribution and the spatial distribution of iron nanoparticles on the support, before and after catalytic testing, (scanning) transmission electron microscopy ((S)TEM) was used. Images were recorded with an FEI Talos F200X transmission electron microscope, operated at 200 kV in bright field (TEM) or dark field mode (STEM). The samples were prepared on Formvar carbon film, 200 mesh copper grids. The samples were dispersed in pure ethanol, sonicated, and drop casted on the TEM grids.

2.2.3. Ar-Physisorption. Ar-physisorption at −196 °C was carried out on a Micromeritics TriStar 3000 to determine the specific surface area and pore volume of the parent zeolite. Prior to measurement, the material was dried in a nitrogen flow at 300 °C for 16 h.

2.2.4. Temperature-Programmed Ammonia Desorption. Temperature-programmed ammonia desorption (NH_3-TPD) was done to determine the total amount of acid sites on all catalysts with around 50 mg per sample. Drying was carried out with a heating ramp of 10 °C/min until a temperature of 600 °C was reached for 15 min. The samples were cooled down to 100 °C and ammonium gas (10% NH_3 in He) was dosed to the samples. Ammonium desorption was performed by heating again to 600 °C with 10 °C/min.

2.2.5. Pyridine Infrared Spectroscopy. Pyridine Infrared (IR) measurements were done as an addition to the NH_3-TPD. Around 20 mg of sample was pelletized into IR pellets with a diameter of 1.3 cm. IR spectra were taken with a PerkinElmer System 2000 instrument in the spectral range of 4000−400 cm^{-1} (32 spectra were acquired per sample). Background spectra were recorded on an empty cell under vacuum ($\sim 10^{-5}$ mbar). Drying of the pellet was done under the same pressure with a heat ramp of 5 °C/min until a temperature of 350 °C was reached and held for 3 h. The samples were cooled down to room temperature and pyridine gas was introduced ($p_{Py} \approx 15$ mbar) for 30 min. Thereafter, desorption was performed at vacuum ($\sim 10^{-5}$ mbar) by heating with a heat ramp of 5 °C/min until a temperature of 150 °C was reached and held for 30 min. The pyridine was desorbed by heating up to 150 °C while taking spectra every 25 °C. When 150 °C was reached, the temperature was held for 30 min and spectra were recorded every 10 min. Complete desorption of the pyridine was achieved by heating to 550 °C (5 °C/min) and maintaining that temperature for 2 h. The acid sites were calculated following methods originating from both Emeis et al. and Hernández-Giménez, A. et al.[48−50]

2.2.6. Thermogravimetric Analysis Mass Spectrometry (TGA-MS). TGA was performed to analyze the organic ligands present on the particles. The ligand content of samples ZSM-5 (support), Fe/Z, and FeP/Z was measured using a PerkinElmer TGA8000, hyphenated with a Hiden HPR-20 mass spectrometer. Catalysts were heated from 30 °C to 800 °C (5 °C/min) in 20% O_2 in Ar (16 mL/min). Additionally, ZSM-5 treated with the organic liquids using the same procedure as that in section 2.1.2. (Attachment of Fe-NP onto H-ZSM-5) without suspended iron particles present was measured. Lastly, Fe/Z was measured as well by using a reduction procedure (5 °C/min to 350 °C for 2 h, 5% H_2 in Ar, 25 mL/min) to find if the ligands were removed during the in situ reduction in the FTO reaction. To verify the removal of the ligands, the reduced Fe/Z was again measured by heating from 30 °C to 800 °C (5 °C/min) in 20% O_2 in Ar (16 mL/min).

2.3. Catalytic Performance. To examine the catalytic performance of the synthesized catalysts in the conversion of synthesis gas to olefins and aromatics, experiments were performed at 1 and 10 bar pressure.

2.3.1. Catalytic Performance at 1 bar. The catalytic performance was investigated at 1 bar by loading 20 mg of Fe-NP supported on zeolite (sieve fraction of 75−150 μm) diluted with 150 mg silicon carbide (sieve fraction of 212−425 μm) into a quartz reactor. After in situ reduction at 350 °C (5 °C/min) in a flow of 15 mL/min of hydrogen in nitrogen (2:1

https://dx.doi.org/10.1021/acscatal.9b04380
ACS Catal. 2020, 10, 1913−1922

v/v, resulting GHSV = 12 500 h^{-1}) for 2 h, a carburization step was performed at 290 °C (5 °C/min) in a flow of 6 mL/min of synthesis gas ($CO:H_2$ = 1 v/v, resulting GHSV = 5000 h^{-1}) for 1 h. The reaction was carried out at 340 °C (5 °C/min) in a flow of 6 mL/min of synthesis gas ($CO:H_2$ = 1 v/v, resulting GHSV = 5000 h^{-1}) for 16 h. The hydrocarbon products were analyzed with an online-gas chromatograph (Varian 430-GC) equipped with a flame ionization detector. CO conversion was calculated from the formation of hydrocarbon from synthesis gas. Selectivities were calculated as hydrocarbon distribution on carbon atom basis (CO_2 free). A CO_2 selectivity of 40−45% is expected which is around the thermodynamic limit under these conditions. In this specific gas chromatograph, lower olefins and paraffins could not be separated. Therefore, the C_2−C_4 selectivity will always be shown as a combined number of both the olefins and the paraffins. The activity was calculated as iron time yield (FTY) which is defined as moles of CO being converted per gram of iron per second.

2.3.2. Catalytic Performance at 10 bar. The experiments performed at 10 bar were carried out in a 16-channel high throughput setup (Avantium Flowrence). Fifteen mg of the Fe-NP supported on zeolite (sieve fraction of 75−150 μm) was diluted with 100 mg silicon carbide (sieve fraction of 212−425 μm) and loaded into stainless steel reactors with 2.6 mm inner diameter. After in situ reduction in a flow of 30% H_2 in He (v/v, resulting GHSV = 6900 h^{-1}) at 350 °C and 1 bar for 2 h, a carburization step was performed at 290 °C (5 °C/min) and 1 bar for 1 h in a flow of 3.75 mL_{STP}/min synthesis gas ($CO:H_2:He$ = 6:12:1 v/v/v, resulting GHSV = 4100 h^{-1}). Reaction conditions were applied by increasing the reactor temperature to 340 °C with 5 °C/min and increasing the pressure to 10 bar in a flow of 3.75 mL_{STP}/min synthesis gas ($CO:H_2:He$ = 6:12:1 v/v/v, resulting GHSV = 4100 h^{-1}). The reaction products were analyzed by an online gas chromatograph (Agilent 7890A) equipped with a flame ionization detector and a thermal conductivity detector. For the CO conversion in the high-pressure experiments, the conversion toward hydrocarbons and the formation of CO_2 in the WGS was taken into account. Selectivities were calculated as distribution within hydrocarbon on carbon atom basis (CO_2 free).

3. RESULTS AND DISCUSSION

3.1. Characterization of the Catalysts. Iron oxide nanoparticles (Fe-NP) of 6 nm were synthesized according to a previously published method.[41,43] Figure 1A shows a transmission electron micrograph of the colloidal particles synthesized with organic oleic acid and oleylamine ligands. The organic ligands separated the iron oxide particles by 2 nm when dried on the transmission electron microscopy (TEM) grid, which is associated with the length of one oleic acid or oleylamine ligand.[51,52] These Fe-NP were used in an inorganic ligand exchange step to add Na + S promoters, following a procedure mentioned in previous research[45,46] (FeP-NP). Notably, the particle size was unaffected after the inorganic ligand exchange, as can be observed in the histograms but particles came in close proximity to one another on the TEM grid (Figure 1B). The shortening of distance was assigned to stronger particle−particle interactions originating from the charge stabilizing ligands compared to the steric stabilizing organic ligands in Fe-NP and the replacement of long oleic acid and oleylamine ligands by small Na/S ligands.[52]

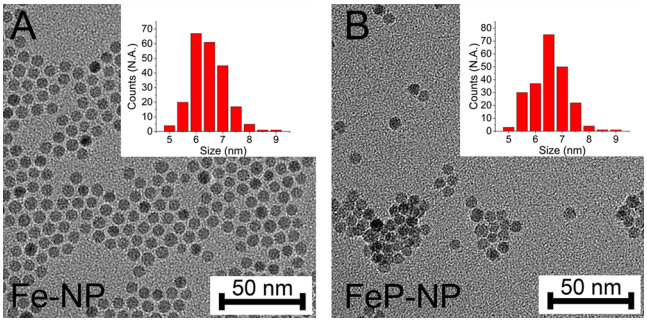

Figure 1. Electron micrographs of the colloidal iron oxide nanoparticles with organic ligands (A) and inorganic ligands (B) dried on a TEM grid. The insets show the histogram of the size of the particles with a number-average particle size of 6 nm.

The Fe-NP in toluene and the FeP-NP in methanol were attached to an H-ZSM-5 zeolite producing Fe/Z and FeP/Z, respectively (Figure 2A,B) (Sample codes and descriptions are summarized in Table S1). The micropore dimensions of H-ZSM-5 zeolites are 0.53 × 0.58 nm^2,[53] implying that the colloidal particles of 6 nm could not enter the micropores, but attached to the external surface of the zeolite crystals. The bare H-ZSM-5 material had a micropore surface area of 365 m^2/g and an external surface area of 50 m^2/g (obtained from T-plot) as obtained from argon physisorption, see Figure S2 in the SI. As the external surface area was relatively small, the particle to particle distances were small, especially compared to colloidal particles with similar weight loading on carbon nanotubes from previous literature,[41,43] which had an external surface area of 230 m^2/g. The particle size of the Fe-NP was not significantly affected by the attachment to the support, see insets in Figure 2. FeP/Z in Figure 2B displayed chains of particles probably because of the small ligand sizes which enabled magnetic interactions of maghemite or magnetite domains. The inorganic ligand exchange of Fe/Z to obtain Fe/Z-P did not alter the particle size and distribution, as can be seen in Figure 2C.

Inductively coupled plasma atomic emission spectroscopy (ICP-AES) was used to determine the weight loading of iron, sodium and sulfur on the catalysts, see Table 1. The iron weight loading was close to 3 wt % in all samples, however, the sodium and sulfur content varied per catalyst. As the sulfur content was relatively low in the catalysts and close or below to the detection limit of the apparatus, the ICP values for sulfur should be considered only as indicative values.

Previous research gave an indication that for colloidal Fe-NP-based catalysts an Na/Fe ratio of 0.09−0.12 at/at would be optimal for a high CO conversion and high C_2−C_4 olefin selectivity.[44,54] Considerably higher Na/Fe ratios resulted in a decrease in activity by overpromotion of the catalyst.[54] The sodium to iron ratio in this study was relatively high (Na/Fe = 0.17−0.21 at/at) on both of the promoted catalysts, most likely overpromoting both systems. In addition, there is a possibility that the excess of sodium could be located on the Brønsted acid (BAS) sites of the zeolite, blocking the acid sites and therefore deactivating the zeolite.

3.2. Removal of Promoter Excess. To remove the excess of promoters from the iron nanoparticles and zeolite, an additional washing step using ion exchange was applied with ammonium nitrate, creating the following catalysts: Fe/Z-W, FeP/Z-W and Fe/Z-P-W. TEM images of the catalysts obtained through the washing step are shown in Figure S3.

https://dx.doi.org/10.1021/acscatal.9b04380
ACS Catal. 2020, 10, 1913−1922

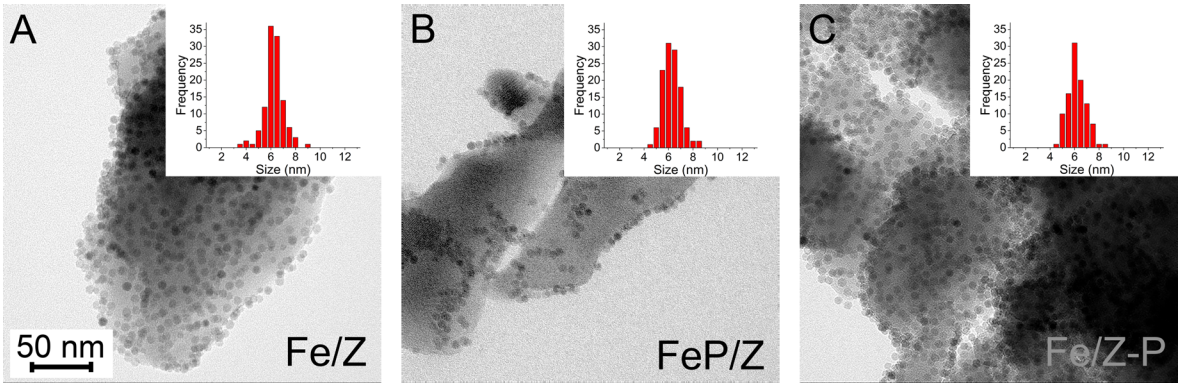

Figure 2. Electron micrographs of the iron oxide nanoparticles attached to H-ZSM-5 with organic ligands, Fe/Z (A). Na+S ligand exchange performed before attachment of Fe to the zeolite, FeP/Z (B) and Na+S ligand exchanged after attaching, Fe/Z-P (C). Histograms of particle sizes inserted in the top, right show the narrow Fe particle size distribution and average particle size of 6 nm independent of the synthesis method.

Table 1. Particle Size, Standard Deviation, and Weight Loading of All Catalysts[a]

sample name	particle size (nm)	Fe (wt %)	Na/Fe (at/at)[b]	S/Fe (at/at)[b]	Na/BAS (mol/mol)[c]
Fe/Z	6.0	3.3	<dl	<dl	ND
Fe/Z-W	6.2	3.2	<dl	<dl	ND
FeP/Z	6.0	2.8	0.21	0.03	0.79
FeP/Z-W	5.9	2.7	<dl	<dl	ND
Fe/Z-P	6.0	3.7	0.17	0.05	0.73
Fe/Z-P-W	6.0	3.2	0.14	0.03	0.56

[a]No size change was found when attaching the Fe-NP to the zeolite support, or when washing and calcining the catalysts. The weight loading was determined by ICP-AES and showed all catalysts had similar iron weight loadings. [b]<d.l. the detection limit for sulfur was 0.07 wt % and for sodium 0.02 wt %. [c]N.D. = not determined. BAS = Bronsted Acid Sites.

No significant change in particle size and hardly in iron content were observed from TEM and ICP measurements (Table 1). ICP indicated that due to the washing step the sodium on FeP/Z was almost entirely removed from the catalyst. In the Fe/Z-P catalyst, however, some sodium was removed but most was retained, and hence this catalyst was more comparable with active catalysts from previous research.[44,54]

To get an indication of whether sodium was specifically attached to the iron and/or to the Brønsted acid sites (BAS), temperature-controlled desorption NH_3-TPD and pyridine IR were measured, see Figures S4–S9 in the SI. The NH_3-TPD results could only be used as indicative values as the ammonia did not specifically bind to only the acid sites of the zeolite but also the iron (-oxide or -hydroxide) sites.[55] Therefore, pyridine IR was used to obtain a quantity for the BAS, see Figures S6–S9 in the SI. Using pyridine IR, a peak indicating the BAS can be found at 1543 cm^{-1} while the peak indicating the Lewis acid sites (LAS) are at 1455 cm^{-1}. The peak at 1490 cm^{-1} originates from BAS in the vicinity of LAS.[50] To confirm that the pyridine did not absorb on the iron particles, measurements were performed on SiO_2 and Fe-NP/SiO_2, see Figures S6 and S7. No pyridine was absorbed by the silica itself, as indicated by Figure S6. The Fe-NP did absorb pyridine as a peak was found at 1450 cm^{-1} to indicate LAS, see Figure S7. However, this pyridine was weakly bound to the iron particles and desorbed before a temperature of 150 °C was reached (the temperature used to calculate the number of BAS and LAS), confirming that this absorbed pyridine was of no influence on the calculations done for the acid site concentrations.

By integrating the BAS peak in Figure S8 it was found that the BAS in the H-ZSM-5 zeolite was 0.14 mmol/g. From this number and the ICP values given in Table 1 (assuming that all sodium would have been incorporated in the zeolite) the maximum amount of blocked acid sites was calculated. It was established that if all sodium was located on the zeolite a maximum of 79% of all the BAS on the zeolite could be deactivated. However, when comparing the concentration of the BAS in Figure S9, it was noticeable that all the catalysts remained relatively similar to the parent zeolite implying that the Na was mostly situated on the Fe-NP. Therefore, even though sodium could have deactivated 79% of the BAS, pyridine IR showed that acidity remained unchanged upon addition of promoters via ligand exchange, which shows that the ligands have a strong affinity toward the iron particles.

3.3. Synthesis Gas Conversion. To assess the activity and selectivity toward methane, C_2–C_4 fraction and aromatics, the catalyst performance was observed under Fischer–Tropsch to Olefins (FTO) conditions to convert synthesis gas to olefins and aromatics (Figures 3 and 4). The activity is shown as iron time yield (FTY), i.e., the number of moles of CO converted per gram of iron per second. The promoted and unpromoted catalysts showed low activity, as can be observed in Figure 3A, and low CO conversion as observed in Table S2. To make sure

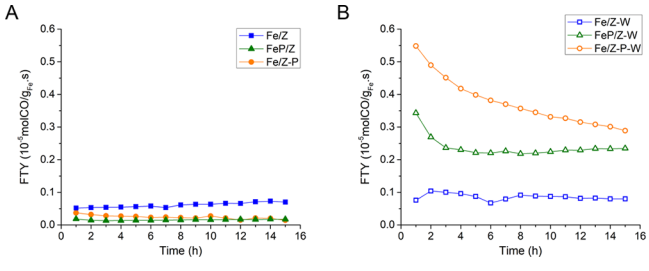

Figure 3. Iron time yield (FTY; defined as moles of CO being converted per gram of iron per second) at 1 bar and 340 °C with H_2:CO ratios of 1 plotted as a function of time on stream for as-synthesized catalysts (A) and washed catalysts (B). As can be observed in graph (A), (un)promoted as-synthesized catalysts had a low activity due to overpromotion compared to the washed catalysts (B). Adding promoters and afterward removing excess Na led to active catalysts. All catalysts were operated at CO conversions in the range of 3–5% conversion.

https://dx.doi.org/10.1021/acscatal.9b04380
ACS Catal. 2020, 10, 1913–1922

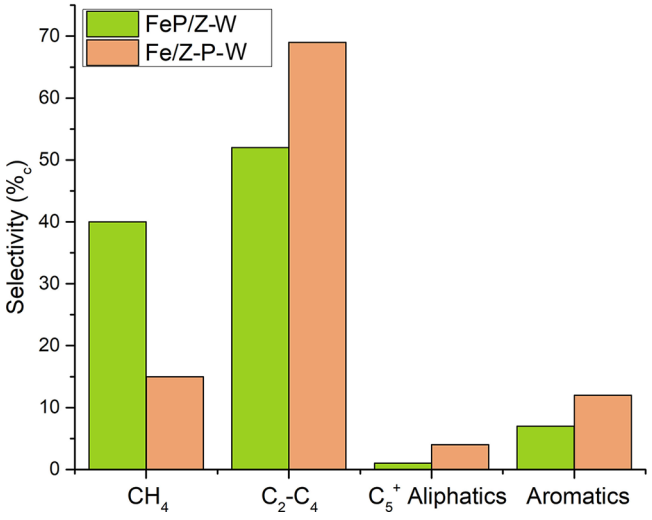

Figure 4. Catalyst selectivity of H-ZSM-5 supported iron catalysts (FeP/Z-W in green and Fe/Z-P-W in orange) under FTO conditions at 340 °C, 1 bar, H_2/CO = 1 (v/v), GHSV: 4 200 h^{-1}, TOS = 15 h. The methane selectivity of FeP/Z-W was high compared to Fe/Z-P-W as, according to ICP, most of the promoted Na/S was removed during the washing step. Both catalysts produced aromatics and Fe/Z-P-W formed a relatively high amount of C_2-C_4 products.

this was not due to any residual organic ligands blocking the active iron sites, thermogravimetric analysis coupled with mass spectrometry (TGA-MS) was carried out, see Figure S10. It was found that Fe/Z retained some of the ligands after the washing and drying steps, but these were removed during the in situ reduction done prior to catalysis. As discussed earlier, the promoted catalysts were likely overpromoted and did not show activity due to the high sodium content.[44] An equally low CO conversion was found in the washed Fe/Z-W catalyst (Figure 3B), clearly indicating that without promoters no activity is found. However, when the promoted catalysts were washed with the ammonium nitrate solution to remove the excess of promoters, the activity was recovered, see Figure 3B. Interestingly, FeP/Z-W retained activity after washing, although ICP indicated that sodium content was below Na/Fe = 0.03 at/at. Most probably small fractions of sodium, undetectable for ICP, had not been removed and still acted as promoters for this catalyst. After 4 h on stream, catalyst FeP/Z-W seemed to have reached equilibrium and was stable up to 16 h on stream. Fe/Z-P-W however, showed activity loss during the 16 h on stream, not reaching equilibrium within this time. As all other catalysts had relatively low activity, it was difficult to assess if these catalysts stayed stable, or merely inactive. It is well-known that the active phase in Fischer–Tropsch catalysis are iron carbides. From previous literature it is apparent that using Na and S promote carbide formation and therefore activity during FT. Thus, it was assumed that the promoters in all washed catalysts facilitated the formation of iron carbides and hence a higher activity than Fe/Z-W.[23,24,28,41]

The methane, aromatics, C_2-C_4 (olefins and paraffins), and C_{5+}-aliphatics selectivities were only plotted for the FeP/Z-W and Fe/Z-P-W catalysts, as these showed CO conversions to

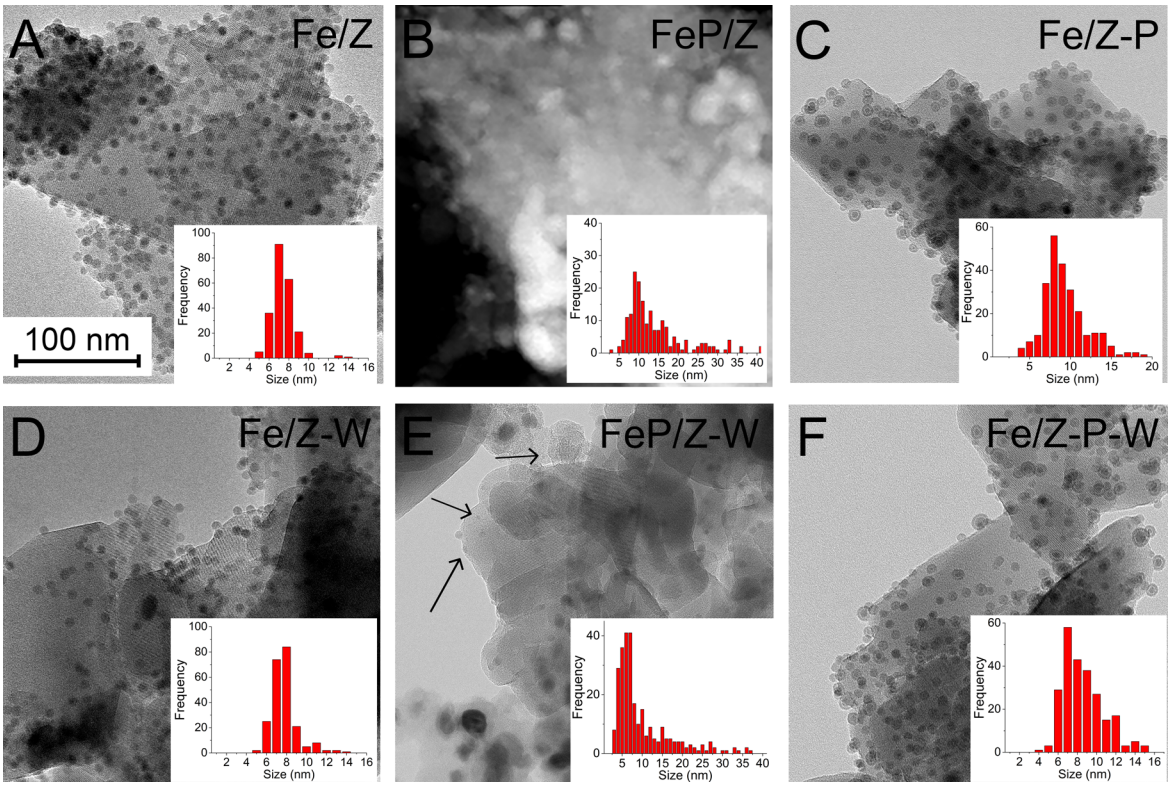

Figure 5. TEM images of all 1 bar used catalysts. (A–C) Fe/Z (A), FeP/Z (B), and Fe/Z-P (C). (D–F) Fe/Z (D), FeP/Z (E), and Fe/Z-P (F). The unpromoted catalysts (Fe/Z and Fe/Z-W) showed little particle growth. Catalysts that had been promoted after attachment (Fe/Z-P and Fe/Z-P-W) showed particle growth up to 20 nm. Spent FeP/Z and FeP/Z-W catalysts showed next to larger particles also smaller particles (see arrows) compared to the fresh catalyst with a distribution that is skewed to larger sizes, as can be seen from the inset histograms. A large fraction of the original 6 nm particles had shrunk to <5 nm particles or grown to particles >10 nm.

https://dx.doi.org/10.1021/acscatal.9b04380
ACS Catal. 2020, 10, 1913–1922

allow reliable measurement of selectivities, see Figure 4. The C_2-C_4 selectivities are given as a sum of paraffins and olefins. A high olefins/paraffins ratio of ~10 mol/mol is expected for the washed catalysts, as at low pressures relatively small amounts of olefins undergo secondary hydrogenation reactions.[28] The methane selectivity gives an indication of the presence of sodium and sulfur promoters on the iron particles, as these promoters significantly decrease the methane selectivity.[23] FeP/Z-W had a methane selectivity of 40%$_C$, in agreement with the low Na/S content obtained from ICP further indicating that most of the Na and S had been removed. Fe/Z-P-W seemed to have retained the promoter effect, enough to lower the methane selectivity to 15%$_C$. This catalyst also obtained a relatively high C_2-C_4 selectivity and a low selectivity toward C_{5+}-aliphatics. The selectivities toward C_4-isomers and aromatics is shown in Table S2 which are similar for both active catalysts. Both washed catalysts produced aromatics at 1 bar but as FeP/Z-W had a relatively low Na content, it showed a high selectivity toward methane and a lower selectivity toward olefins and aromatics. The methane selectivity is a good measure for Na and S depletion from the iron phase,[32] and hence it was tracked over time (Figure S11 in the SI) to infer if migration of sodium or sulfur species to the ZSM-5 support occurred. At 1 bar pressure, no change with time of the methane selectivity was found, indicating no migration of sodium and sulfur species. The deactivation of FeP/Z-W is limited but that of Fe/Z-P-W is extensive which can be explained by the different particle−particle distances of the fresh catalysts (Figure 2B,C). The smaller interparticle distances of FeP/Z-W may facilitate sintering most probably already during the reduction leading to lower activity but higher stability whereas with Fe/Z-P-W the sintering during reduction is limited leading to high initial activity but more particle growth with concomitant deactivation during FT.

Additionally, the catalytic performance was established for all catalysts at medium pressure (10 bar) and reported in Table S3. The CO conversions of the washed catalysts were similar (between 10 and 15%). The activity increase after washing the catalysts was also seen at medium pressure. Furthermore, Fischer−Tropsch at medium pressure led to a significant increase in methane formation and a concomitant decrease of aromatics selectivity pointing to a higher hydrogenation activity.[28] The FT activity of the promoted catalysts was similar to promoted colloidal particles supported on carbon nanotubes as reported in literature.[44]

3.4. Analysis of the Used Catalysts. The used catalysts of the 1 and 10 bar experiment were analyzed using TEM (Figures 5 and S12 and Table S3 in the SI). At 1 bar, notably, particles were remarkably stable in the unpromoted catalyst (Figure 5A,D), especially considering the initial small particle−particle distances. Growth was observed in the promoted catalysts, particularly FeP/Z, in line with previous studies showing that if Na and S are present, this accelerates particle growth.[24] A combination of factors could have caused this growth, namely a large number of promoters and altered particle-support interaction as well as a less homogeneous distribution of particles in the fresh catalyst due to the short ligands. This resulted in particle growth to at least twice the initial diameter, as can be observed in Figure 5B. Scanning-transmission electron microscopy (STEM) images were made for this catalyst to better observe the contrast between the large iron particles and the zeolite. Moreover, when applying high-pressure conditions, the growth of FeP/Z became even more evident (Figure S12E).

At 10 bar, Fe/Z-P (Figure S12C) grew into a bimodal size distribution at showing that the promoters have a large influence on the catalyst stability, which is in agreement with previous work on carbon nanofibers.[24] In this previous research on colloidal particles attached to carbon performed at 10 bar, a bimodal particle size distribution was seen as well. The increased growth rate was therefore attributed to the higher pressure used in catalysis.[44] This is supported by Figure S1, where 10 bar catalysis did yield particle sizes comparable with the previously discussed colloidal particles on carbon.

Furthermore, in Figures 5E and S13 it is observed that the particle size distribution in FeP/Z-W ranged from particles smaller than the fresh catalyst's size (<5 nm) to larger (>10 nm) particles. This strongly indicates that the growth mechanism is dominated by the Ostwald ripening process.[56] In previous studies, DFT calculations found that elevated temperatures and the presence of CO can induce subcarbonyl species with high mobility, making Fischer−Tropsch catalysts prone to Ostwald ripening.[57−59] To our knowledge, no similar results have been reported with evidence of particle shrinking after catalysis for iron FT catalysis. These data indicate that sintering of the colloidal particles goes through the Ostwald ripening process where Fe subcarbonyls most likely play an important role. Furthermore, as pointed out in previous research, sulfur might accelerate the production of iron pentacarbonyl species which indicates that the S promoters enhance the growth rather than suppress it.[60]

4. CONCLUSIONS

In summary, using colloidal particles attached to an H-ZSM-5 support resulted in a uniform metal particle distribution on the external surfaces of the zeolite crystals (Fe/Z) even if these particles were promoted afterward with Na and S (Fe/Z-P), while at the same time displaying a narrow particle size distribution when organic ligands were used. When inorganic ligands were present before attaching the particles to the zeolite surface (FeP/Z), particles were less uniformly distributed due to their small ligand sizes but still showed a narrow particle size distribution. The large amount of Na and S in both Fe/Z-P and FeP/Z resulted in low catalyst activity, as both catalysts were overpromoted. The promoter amount was lowered with an additional washing step using ammonium nitrate enhancing the activity for both catalysts. However, washing the FeP/Z catalyst caused the amount of promoters to drop below the detection limit of ICP, thus loosing promotion effect and therefore obtaining a high methane selectivity. After washing Fe/Z-P showed a low selectivity toward methane and the formation of aromatics. Pyridine IR showed that the zeolite retained acidity using the colloidal ligand exchange method even though the zeolite was in direct contact with the promoter solution. Clearly, this ligand exchange is a promising method to obtain active and selective iron on zeolite catalysts, because it enables the steering of promoters to the iron particles instead of on the zeolite acid sites.

Additionally, it was confirmed again that adding Na and S promoters accelerated particle growth during catalysis. During the analysis of the FeP/Z-W used catalyst, it was found that the particle size had both increased and decreased, suggesting an Ostwald ripening process accelerated by the added promoters. Therefore, this research additionally shows that due to the advantageous narrow particle size distribution, colloids can be

https://dx.doi.org/10.1021/acscatal.9b04380
ACS Catal. 2020, 10, 1913−1922

used to investigate particle growth and that using ligand exchange directs the promoters specifically toward the iron particles instead of reducing zeolite acidity.

■ ASSOCIATED CONTENT

Supporting Information

The Supporting Information is available free of charge at https://pubs.acs.org/doi/10.1021/acscatal.9b04380.

Figures S1−S11, including ammonia TPD measurements (bar graphs of the data and the spectra), physisorption plots, and TEM images of washed and used catalysts at 10 bar and pyridine IR spectra; Table S1, the explained nomenclature; and Tables S2 and S3, the data from catalyst performance at 1 and 10 bar including the CO conversion, FTY, and selectivities (PDF)

■ AUTHOR INFORMATION

Corresponding Author

K. P. de Jong − *Utrecht University, Utrecht, The Netherlands;* orcid.org/0000-0002-9773-8110; Email: k.p.dejong@uu.nl

Other Authors

N. A. Krans − *Utrecht University, Utrecht, The Netherlands;* orcid.org/0000-0002-3764-3187

J. L. Weber − *Utrecht University, Utrecht, The Netherlands*

W. van den Bosch − *Utrecht University, Utrecht, The Netherlands*

J. Zečević − *Utrecht University, Utrecht, The Netherlands*

P. E. de Jongh − *Utrecht University, Utrecht, The Netherlands;* orcid.org/0000-0002-2216-2620

Complete contact information is available at: https://pubs.acs.org/10.1021/acscatal.9b04380

Author Contributions

The manuscript was written through the contributions of all authors. All authors have given approval to the final version of the manuscript.

Author Contributions

†These authors contributed equally to this work.

Notes

The authors declare no competing financial interest.

■ ACKNOWLEDGMENTS

We acknowledge the European Research Council, EU FP7 ERC Advanced Grant no. 338846. This work was supported by The Netherlands Center for Multiscale Catalytic Energy Conversion (MCEC), an NWO Gravitation program funded by the Ministry of Education, Culture and Science of the government of The Netherlands. J.Z. acknowledges financial support by The Netherlands Organization for Scientific Research (NWO), Veni Grant no. 722.015.010. Remco Dalebout is thanked for argon physisorption measurements and Coen Mulder is thanked for ICP-AES measurements. Dennie Wezendonk is thanked for the TGA-MS measurements. Peter van den Brink (Shell) is thanked for providing insight and expertise that assisted the research.

■ REFERENCES

(1) Dybkjaer, I. Tubular Reforming and Autothermal Reforming of Natural Gas - An Overview of Available Processes. *Fuel Process. Technol.* **1995**, *42*, 85−107.

(2) Hernández, J. J.; Aranda-Almansa, G.; Serrano, C. Co-Gasification of Biomass Wastes and Coal-Coke Blends in an Entrained Flow Gasifier: An Experimental Study. *Energy Fuels* **2010**, *24*, 2479−2488.

(3) Hernández, J. J.; Aranda-Almansa, G.; Bula, A. Gasification of Biomass Wastes in an Entrained Flow Gasifier: Effect of the Particle Size and the Residence Time. *Fuel Process. Technol.* **2010**, *91*, 681−692.

(4) Luo, S.; Zeng, L.; Xu, D.; Kathe, M.; Chung, E.; Deshpande, N.; Qin, L.; Majumder, A.; Hsieh, T. L.; Tong, A.; Sun, Z.; Fan, L. S. Shale Gas-to-Syngas Chemical Looping Process for Stable Shale Gas Conversion to High Purity Syngas with a H_2:CO ratio of 2:1. *Energy Environ. Sci.* **2014**, *7*, 4104−4117.

(5) Wender, I. Reactions of Synthesis Gas. *Fuel Process. Technol.* **1996**, *48*, 189−297.

(6) Khodakov, A. Y.; Chu, W.; Fongarland, P. Advances in the Development of Novel Cobalt Fischer−Tropsch Catalysts for Synthesis of Long-Chain Hydrocarbons and Clean Fuels. *Chem. Rev.* **2007**, *107*, 1692−1744.

(7) Bezemer, G. L.; Bitter, J. H.; Kuipers, H. P. C. E.; Oosterbeek, H.; Holewijn, J. E.; Xu, X.; Kapteijn, F.; Van Dillen, A. J.; De Jong, K. P. Cobalt Particle Size Effects in the Fischer - Tropsch Reaction Studied with Carbon Nanofiber Supported Catalysts. *J. Am. Chem. Soc.* **2006**, *128*, 3956−3964.

(8) Van Den Berg, R.; Prieto, G.; Korpershoek, G.; Van Der Wal, L. I.; Van Bunningen, A. J.; Lægsgaard-Jørgensen, S.; De Jongh, P. E.; De Jong, K. P. Structure Sensitivity of Cu and CuZn Catalysts Relevant to Industrial Methanol Synthesis. *Nat. Commun.* **2016**, *7*, 13057.

(9) Jiao, F.; Li, J.; Pan, X.; Xiao, J.; Li, H.; Ma, H.; Wei, M.; Pan, Y.; Zhou, Z.; Li, M.; Miao, S.; Li, J.; Zhu, Y.; Xiao, D.; He, T.; Yang, J.; Qi, F.; Fu, Q.; Bao, X. Selective Conversion of Syngas to Light Olefins. *Science* **2016**, *351*, 1065−1068.

(10) Cheng, K.; Zhou, W.; Kang, J.; He, S.; Shi, S.; Zhang, Q.; Pan, Y.; Wen, W.; Wang, Y. Bifunctional Catalysts for One-Step Conversion of Syngas into Aromatics with Excellent Selectivity and Stability. *Chem.* **2017**, *3*, 334−347.

(11) Sartipi, S.; Parashar, K.; Makkee, M.; Gascon, J.; Kapteijn, F. Breaking the Fischer−Tropsch Synthesis Selectivity: Direct Conversion of Syngas to Gasoline over Hierarchical Co/H-ZSM-5 Catalysts. *Catal. Sci. Technol.* **2013**, *3*, 572−575.

(12) Zhu, Y.; Pan, X.; Jiao, F.; Li, J.; Yang, J.; Ding, M.; Han, Y.; Liu, Z.; Bao, X. Role of Manganese Oxide in Syngas Conversion to Light Olefins. *ACS Catal.* **2017**, *7*, 2800−2804.

(13) Li, N.; Jiao, F.; Pan, X.; Ding, Y.; Feng, J.; Bao, X. Size Effects of ZnO Nanoparticles in Bifunctional Catalysts for Selective Syngas Conversion. *ACS Catal.* **2019**, *9*, 960−966.

(14) Cheng, K.; Gu, B.; Liu, X.; Kang, J.; Zhang, Q.; Wang, Y. Direct and Highly Selective Conversion of Synthesis Gas into Lower Olefins: Design of a Bifunctional Catalyst Combining Methanol Synthesis and Carbon-Carbon Coupling. *Angew. Chem., Int. Ed.* **2016**, *55*, 4725−4728.

(15) Zhou, W.; Shi, S.; Wang, Y.; Zhang, L.; Wang, Y.; Zhang, G.; Min, X.; Cheng, K.; Zhang, Q.; Kang, J.; Wang, Y. Selective Conversion of Syngas to Aromatics over a Mo-ZrO_2/H-ZSM-5 Bifunctional Catalyst. *ChemCatChem* **2019**, *11*, 1681−1688.

(16) Wilhelm, D. J.; Simbeck, D. R.; Karp, A. D.; Dickenson, R. L. Syngas Production for Gas-to-Liquids Applications: Technologies, Issues and Outlook. *Fuel Process. Technol.* **2001**, *71*, 139−148.

(17) Sartipi, S.; Van Dijk, J. E.; Gascon, J.; Kapteijn, F. Toward Bifunctional Catalysts for the Direct Conversion of Syngas to Gasoline Range Hydrocarbons: H-ZSM-5 Coated Co Versus H-ZSM-5 Supported Co. *Appl. Catal., A* **2013**, *456*, 11−22.

(18) Hernández Mejía, C.; Van Deelen, T. W.; De Jong, K. P. Activity Enhancement of Cobalt Catalysts by Tuning Metal-Support Interactions. *Nat. Commun.* **2018**, *9*, 1−8.

(19) Xie, J.; Yang, J.; Dugulan, A. I.; Holmen, A.; Chen, D.; De Jong, K. P.; Louwerse, M. J. Size and Promoter Effects in Supported Iron Fischer−Tropsch Catalysts: Insights from Experiment and Theory. *ACS Catal.* **2016**, *6*, 3147−3157.
(20) Oschatz, M.; Krans, N.; Xie, J.; De Jong, K. P. Systematic Variation of the Sodium/Sulfur Promoter Content on Carbon-Supported Iron Catalysts for the Fischer−Tropsch to Olefins Reaction. *J. Energy Chem.* **2016**, *25*, 985−993.
(21) Cheng, K.; Ordomsky, V. V.; Legras, B.; Virginie, M.; Paul, S.; Wang, Y.; Khodakov, A. Y. Sodium-Promoted Iron Catalysts Prepared on Different Supports for High Temperature Fischer−Tropsch Synthesis. *Appl. Catal., A* **2015**, *502*, 204−214.
(22) Xu, J.-D.; Chang, Z.-Y.; Zhu, K.-T.; Weng, X.-F.; Weng, W.-Z.; Zheng, Y.-P.; Huang, C.-J.; Wan, H.-L. Effect of Sulfur on α-Al_2O_3-Supported Iron Catalyst for Fischer−Tropsch Synthesis. *Appl. Catal., A* **2016**, *514*, 103−113.
(23) Torres Galvis, H. M.; Koeken, A. C. J.; Bitter, J. H.; Davidian, T.; Ruitenbeek, M.; Dugulan, A. I.; De Jong, K. P. Effects of Sodium and Sulfur on Catalytic Performance of Supported Iron Catalysts for the Fischer−Tropsch Synthesis of Lower Olefins. *J. Catal.* **2013**, *303*, 22−30.
(24) Xie, J.; Torres Galvis, H. M.; Koeken, A. C. J.; Kirilin, A.; Dugulan, A. I.; Ruitenbeek, M.; De Jong, K. P. Size and Promoter Effects on Stability of Carbon-Nanofiber-Supported Iron-Based Fischer−Tropsch Catalysts. *ACS Catal.* **2016**, *6*, 4017−4024.
(25) Jiang, F.; Zhang, M.; Liu, B.; Xu, Y.; Liu, X. Insights into the Influence of Support and Potassium or Sulfur Promoter on Iron-Based Fischer−Tropsch Synthesis: Understanding the Control of Catalytic Activity, Selectivity to Lower Olefins, and Catalyst Deactivation. *Catal. Sci. Technol.* **2017**, *7*, 1245−1265.
(26) Torres Galvis, H. M.; De Jong, K. P. Catalysts for Production of Lower Olefins from Synthesis Gas: A Review. *ACS Catal.* **2013**, *3*, 2130−2149.
(27) Torres Galvis, H. M.; Bitter, J. H.; Khare, C. B.; Ruitenbeek, M.; Dugulan, A. I.; De Jong, K. P. Supported Iron Nanoparticles as Catalysts for Sustainable Production of Lower Olefins. *Science* **2012**, *335*, 835−838.
(28) Weber, J. L.; Dugulan, I.; De Jongh, P. E.; De Jong, K. P. Bifunctional Catalysis for the Conversion of Synthesis Gas to Olefins and Aromatics. *ChemCatChem* **2018**, *10*, 1107−1112.
(29) Karre, A. V.; Kababji, A.; Kugler, E. L.; Dadyburjor, D. B. Effect of Time on Stream and Temperature on Upgraded Products from Fischer − Tropsch Synthesis when Zeolite is Added to Iron-Based Activated-Carbon-Supported Catalyst. *Catal. Today* **2013**, *214*, 82−89.
(30) Karre, A. V.; Kababji, A.; Kugler, E. L.; Dadyburjor, D. B. Effect of Addition of Zeolite to to Iron-Based Activated-Carbon-Supported Catalyst for Fischer−Tropsch Synthesis in Separate Beds and Mixed Beds. *Catal. Today* **2012**, *198*, 280−288.
(31) Ramirez, A.; Chowdhury, A. D.; Dokania, A.; Cnudde, P.; Caglayan, M.; Yarulina, I.; Abou-Hamad, E.; Gevers, L.; Ould-Chikh, S.; De Wispelaere, K.; Van Speybroeck, V.; Gascon, J. Effect of Zeolite Topology and Reactor Configuration on the Direct Conversion of CO_2 to Light Olefins and Aromatics. *ACS Catal.* **2019**, *9*, 6320−6334.
(32) Weber, J. L.; Krans, N. A.; Hofmann, J. P.; Hensen, E. J. M.; Zecevic, J.; De Jongh, P. E.; De Jong, K. P. Effect of Proximity and Support Material on Deactivation of Bifunctional Catalysts for the Conversion of Synthesis Gas to Olefins and Aromatics. *Catal. Today* **2020**, *342*, 161−166.
(33) Meunier, F. C. Bridging the Gap Between Surface Science and Industrial Catalysis. *ACS Nano* **2008**, *2*, 2441−2444.
(34) Sun, B.; Xu, K.; Nguyen, L.; Qiao, M.; Tao, F. Preparation and Catalysis of Carbon-Supported Iron Catalysts for Fischer − Tropsch Synthesis. *ChemCatChem* **2012**, *4*, 1498−1511.
(35) Cheng, K.; Virginie, M.; Ordomsky, V. V.; Cordier, C.; Chernavskii, P. A.; Ivantsov, M. I.; Paul, S.; Wang, Y.; Khodakov, A. Y. Pore Size Effects in High-Temperature Fischer − Tropsch Synthesis over Supported Iron Catalysts. *J. Catal.* **2015**, *328*, 139−150.
(36) Den Breejen, J. P.; Radstake, P. B.; Bezemer, G. L.; Bitter, J. H.; Frøseth, V.; Holmen, A.; De Jong, K. P. On the Origin of the Cobalt Particle Size Effects in Fischer−Tropsch Catalysis. *J. Am. Chem. Soc.* **2009**, *131*, 7197−7203.
(37) Torres Galvis, H. M.; Bitter, J. H.; Davidian, T.; Ruitenbeek, M.; Dugulan, A. I.; De Jong, K. P. Iron Particle Size Effects for Direct Production of Lower Olefins from Synthesis Gas. *J. Am. Chem. Soc.* **2012**, *134*, 16207−16215.
(38) Van Deelen, T. W.; Nijhuis, J. J.; Krans, N. A.; Zečević, J.; De Jong, K. P. Preparation of Cobalt Nanocrystals Supported on Metal Oxides to Study Particle Growth in Fischer−Tropsch Catalysts. *ACS Catal.* **2018**, *8*, 10581−10589.
(39) Ritz, B.; Heller, H.; Myalitsin, A.; Kornowski, A.; Martin-Martinez, F. J.; Melchor, S.; Dobado, J. A.; Juárez, B. H.; Weller, H.; Klinke, C. Reversible Attachment of Platinum Alloy Nanoparticles to Nonfunctionalized Carbon Nanotubes. *ACS Nano* **2010**, *4*, 2438−2444.
(40) Jia, F. C.; Schüth, J. Colloidal Metal Nanoparticles as a Component of Designed Catalyst. *Phys. Chem. Chem. Phys.* **2011**, *13*, 2457−2487.
(41) Krans, N. A.; Van der Feltz, E. C.; Xie, J.; Dugulan, I. A.; Zečević, J.; De Jong, K. P. Attachment of Iron Oxide Nanoparticles to Carbon Nanotubes and the Consequences for Catalysis. *ChemCatChem* **2018**, *10*, 3388−3391.
(42) Krans, N. A.; Ahmad, N.; Alloyeau, D.; De Jong, K. P.; Zečević, J. Attachment of Iron Oxide Nanoparticles to Carbon Nanofibers Studied by *In-Situ* Liquid Phase Transmission Electron Microscopy. *Micron* **2019**, *117*, 40−46.
(43) Casavola, M.; Hermannsdörfer, J.; De Jonge, N.; Dugulan, A. I.; De Jong, K. P. Fabrication of Fischer−Tropsch Catalysts by Deposition of Iron Nanocrystals on Carbon Nanotubes. *Adv. Funct. Mater.* **2015**, *25*, 5309−5319.
(44) Casavola, M.; Xie, J.; Meeldijk, J. D.; Krans, N. A.; Goryachev, A.; Hofmann, J. P.; Dugulan, A. I.; De Jong, K. P. Promoted Iron Nanocrystals Obtained via Ligand Exchange as Active and Selective Catalysts for Synthesis Gas Conversion. *ACS Catal.* **2017**, *7*, 5121−5128.
(45) Nag, A.; Kovalenko, M. V.; Lee, J. S.; Liu, W.; Spokoyny, B.; Talapin, D. V. Metal-free Inorganic Ligands for Colloidal Nanocrystals: S^{2-}, HS^-, Se^{2-}, HSe^-, Te^{2-}, HTe^-, TeS_3^{2-}, OH^-, and NH_2^- as Surface Ligands. *J. Am. Chem. Soc.* **2011**, *133*, 10612−10620.
(46) Van Oversteeg, C. H. M.; Oropeza, F. E.; Hofmann, J. P.; Hensen, E. J. M.; De Jongh, P. E.; De Mello Donega, C. Water-Dispersible Copper Sulfide Nanocrystals via Ligand Exchange of 1-Dodecanethiol. *Chem. Mater.* **2019**, *31*, 541−552.
(47) Hansen, T. W.; Delariva, A. T.; Challa, S. R.; Datye, A. K. Sintering of Catalytic Nanoparticles: Particle Migration or Ostwald Ripening? *Acc. Chem. Res.* **2013**, *46*, 1720−1730.
(48) Hernández-Giménez, A. M.; Ruiz-Martínez, J.; Puértolas, B.; Pérez-Ramírez, J.; Bruijnincx, P. C. A.; Weckhuysen, B. M. Operando Spectroscopy of the Gas-Phase Aldol Condensation of Propanal over Solid Base Catalysts. *Top. Catal.* **2017**, *60*, 1522−1536.
(49) Emeis, C. A. Determination of Integrated Molar Exctinction Coefficients for Infrared Absorption Bands of Pyridine Adsorbed on Solid Acid Catalysts. *J. Catal.* **1993**, *141*, 347−354.
(50) Parry, E. P. An Infrared Study of Pyridine Adsorbed on Acidic Solids. Characterization of Surface Acidity. *J. Catal.* **1963**, *2*, 371−379.
(51) Wang, Z.; Wen, X.-D.; Hoffmann, R.; Son, J. S.; Li, R.; Fang, C.-C.; Smilgies, D.-M.; Hyeon, T. Reconstructing a Solid-Solid Phase Transformation Pathway in CdSe Sanosheets with Associated Soft Ligands. *Proc. Natl. Acad. Sci. U. S. A.* **2010**, *107*, 17119−17124.
(52) Van Der Stam, W.; Rabouw, F. T.; Vonk, S. J. W.; Geuchies, J. J.; Ligthart, H.; Petukhov, A. V.; De Mello Donega, C. Oleic Acid-Induced Atomic Alignment of ZnS Polyhedral Nanocrystals. *Nano Lett.* **2016**, *16*, 2608−2614.
(53) Van Koningsveld, H.; Jansen, J. C.; Van Bekkum, H. The Monoclinic Framework Structure of Zeolite H-ZSM-5. Comparison

https://dx.doi.org/10.1021/acscatal.9b04380
ACS Catal. 2020, 10, 1913−1922

with the Orthorhombic Framework of As-Synthesized ZSM-5. *Zeolites* **1990**, *10*, 235−242.
(54) Oschatz, M.; Krause, S.; Krans, N. A.; Hernández Mejía, C.; Kaskel, S.; De Jong, K. P. Influence of Precursor Porosity on Sodium and Sulfur Promoted Iron/Carbon Fischer−Tropsch Catalysts Derived from Metal−Organic Frameworks. *Chem. Commun.* **2017**, *53*, 10204−10207.
(55) Li, J. P. H.; Adesina, A. A.; Kennedy, E. M.; Stockenhuber, M. A Mechanistic Study of the Knoevenagel Condensation Reaction: New Insights into the Influence of Acid and Base Properties of Mixed Metal Oxide Catalysts on the Catalytic Activity. *Phys. Chem. Chem. Phys.* **2017**, *19*, 26630−26644.
(56) Datye, A. K.; Xu, Q.; Kharas, K. C.; McCarty, J. M. Particle Size Distributions in Heterogeneous Catalysts: What do They Tell us About the Sintering Mechanism? *Catal. Today* **2006**, *111*, 59−67.
(57) Ouyang, R.; Liu, J. X.; Li, W. X. Atomistic Theory of Ostwald Ripening and Disintegration of Supported Metal Particles under Reaction Conditions. *J. Am. Chem. Soc.* **2013**, *135*, 1760−1771.
(58) Janse Van Rensburg, W.; Van Helden, P.; Moodley, D. J.; Claeys, M.; Petersen, M. A.; Van Steen, E. Role of Transient Co-Subcarbonyls in Ostwald Ripening Sintering of Cobalt Supported on γ-Alumina Surfaces. *J. Phys. Chem. C* **2017**, *121*, 16739−16753.
(59) Munnik, P.; Velthoen, M. E. Z.; De Jongh, P. E.; De Jong, K. P.; Gommes, C. J. Nanoparticle Growth in Supported Nickel Catalysts during Methanation Reaction - Larger is Better. *Angew. Chem., Int. Ed.* **2014**, *53*, 9493−9497.
(60) Unger, G.; Schonfelder, H.; Watzenberger, O.; Sterzel, H. J.; Kuhling, K. Preparation of Iron Pentacarbonyl. US Patent 2005/0129605 A1 Jun. 16, 2005.

https://dx.doi.org/10.1021/acscatal.9b04380
ACS Catal. 2020, 10, 1913−1922